Science and Technology Indonesia
e-ISSN:2580-4391 p-ISSN:2580-4405
Vol. 10, No. 3, July 2025

Research Paper

Core Shell Regulations in Co-Precipitation to Regulate Structure and Performance of Single-Crystal NCM622

Siburian Donny Marihot[1], Cheng Yi[1*], Liu Hai[2*], Zhen Jiang He[1], Hua Wenchao[2], Xu Kaihua[2]

[1]*School of Metallurgy and Environment, Central South University, Changsha, 410083, PR China*
[2]*GEM Co., Ltd., Shenzhen, 518133, PR China*
***Corresponding author**: yi.cheng@csu.edu.cn, liuhai@gem.com.cn*

Abstract
The development of single-crystal NCM622 cathodes remains a key focus in lithium-ion battery research due to their stable structure and cycling performance. This study explores the impact of controlled gas environments on particle nucleation and growth, particularly under different nitrogen-to-air (N_2:air) ratios. The optimized condition, hydroxide precursor (HP)-2.5 and single-crystal cathode (SC)-2.5 (N_2 : air = 2.4 : 0.2 during nucleation up to 2.5 μm, followed by N_2 : air = 2.4 : 0 for growth up to 5 μm), facilitates the formation of well-structured particles with a core-shell morphology. This structure enhances sintering efficiency, leading to the successful formation of single-crystal NCM622. Electrochemical evaluations reveal that SC-2.5 exhibits excellent cycling stability, with an initial discharge capacity of 168.48 mAh g^{-1} and a retention of 134.81 mAh g^{-1} after 100 cycles. The capacity retention of 86.32% and Coulombic efficiency of 99.32% indicate minimal degradation and strong electrochemical stability. These findings highlight the importance of controlled synthesis conditions in optimizing lithium-ion battery cathodes for high-performance energy storage applications.

Keywords
Lithium-Ion Batteries, Single-Crystal Cathodes, Core-Shell, Cycling Performance

Received: 13 January 2025, Accepted: 23 April 2025
https://doi.org/10.26554/sti.2025.10.3.895-902

1. INTRODUCTION

Lithium-ion batteries (LIBs) drive modern energy storage systems due to their high energy density, long cycle life, and low self-discharge rate, making them essential in renewable energy storage, electric cars, and portable electronics (Almafie et al., 2024; Chen et al., 2021). Among the key components of LIBs, the cathode material plays a critical role in determining the overall performance of the battery, including its capacity, stability, and lifespan performance (Tajik et al., 2023). In recent years, nickel-rich layered oxides, particularly $LiNi_xCo_yMn_{1-x-y}O_2$ (NCM), have emerged as promising cathode materials due to their high capacity, excellent rate capability, and relatively lower cost compared to alternatives such as lithium cobalt oxide ($LiCoO_2$) (Luo et al., 2022a; Zhu et al., 2024). The tunable composition of NCM cathodes allows for a balance between energy density, structural stability, and cost-effectiveness, making them highly attractive for next-generation LIBs. One of the most studied compositions in the NCM family is NCM622 ($LiNi_{0.6}Co_{0.2}Mn_{0.2}O_2$), which strikes an optimal balance between high capacity (provided by nickel) and structural stability (ensured by cobalt and manganese) (Kim et al., 2019a; Zhu et al., 2023). However, polycrystalline NCM622 cathodes suffer from intrinsic limitations, such as microcrack formation during cycling, which leads to capacity fading and reduced (Oswald et al., 2022; Zhao et al., 2022). To address the issues, various strategies have been explored, including surface coating, elemental doping, and morphological modifications (Ding et al., 2023; Kim et al., 2019b; Lu et al., 2021). Among these, the development of single-crystal NCM622 cathodes has gained significant attention due to their superior mechanical integrity, reduced grain boundaries, and enhanced electrochemical performance (Han et al., 2022; Jo et al., 2022).

Although various studies have investigated single-crystal NCM622 cathode materials, most have primarily focused on surface modification strategies and elemental doping to enhance electrochemical performance. In contrast, few studies have systematically examined the impact of gas atmosphere conditions, such as the N_2 : air ratio, during precursor synthesis on particle morphology, size distribution, and phase stability. However, the gas environment during the co-precipitation process plays a crucial role in determining the final crystal quality,

including both structural parameters and electrochemical properties (Luo et al., 2022b). The lack of comprehensive studies on this aspect highlights a significant research gap in optimizing gas-atmosphere-based approaches for the synthesis of single-crystal NCM622. To address these challenges and research gaps, this study focuses on the co-precipitation synthesis of NCM622 precursors by systematically regulating the N_2 : air ratio. It specifically aims to investigate how variations in the gas atmosphere influence particle formation during precursor synthesis and the subsequent transformation into single-crystal NCM622 cathodes. Through this approach, the study seeks to provide deeper insight into the relationship between synthesis conditions, structural characteristics, and electrochemical performance. The results demonstrate that a well-controlled gas atmosphere can significantly improve particle uniformity, enhance structural stability, and ultimately lead to superior electrochemical performance.

2. EXPERIMENTAL SECTION

2.1 Synthesis of Single-crystal NCM622 Cathodes

The NCM622 was synthesized using the co-precipitation method of Weitong et al. (2023) following the steps below: $NiSO_4$-.$6H_2O$, $CoSO_4.7H_2O$, and $MnSO_4.H_2O$ with a molar ratio of 6:2:2 were dissolved in a reactor tank with 10.5 mol L^{-1} NaOH and 8.5 mol L^{-1} NH_4OH in a 20 L aqueous solution. The pH of the solution was kept at 11.7 for the 7^{th} hour to allow the nucleation of the NCM622 hydroxide precursor (HP). Then followed by slowly lowering the pH to 10.4 to obtain the target pH conditions for the reaction, yielding NCM622 hydroxide precursor with a particle size of 5 μm. Gas condition adjustments were carried out during the synthesis of the NCM622 hydroxide precursor: HP-0 (N_2 : air = 2.4 : 0 (N_2 only), HP-2.5 (N_2 : air = 2.4 : 0.2 up to 2.5 μm, followed by N_2 just from 2.5 μm to 5 μm), and HP-3.75 (N_2 : air = 2.4 : 0.2 up to 3.75 μm, followed by N_2 just from 3.75 μm to 5 μm). The synthesized precursor was rinsed, filtered, and washed using deionized water and dried in a 120°C oven for 24 hours. To form single crystals, HP was mixed with Li_2CO_3 (Li:TM (ternary metals) = 1.12 in molar ratio), sintered at 950°C for 3 hours, and cooled to 820°C for 7 hours under O_2 flow. These samples became single-crystal cathode materials (SC-0, SC-2.5, and SC-3.75).

2.2 Characterization

X-ray diffraction (XRD) was performed using a Rigaku MiniFlex (Cu Kα radiation, 40 kV, 15 mA) to determine the crystal structure, and the data were refined using the Rietveld method in SmartLab Studio II software. The morphology and cross-sectional structure of the cathode materials were observed using scanning electron microscopy (SEM, Thermo Scientific Apreo 2S Hivac). The surface composition was analyzed using energy-dispersive spectroscopy (EDS, Aztec Version 6.0, Oxford, U.K.), ensuring that the penetration depth was suitable for surface analysis. The residual Li_2CO_3 content was measured using inductively coupled plasma (ICP, Thermo Scientific iCAP PRO), while the elemental distribution within particles was examined using an electron probe micro-analyzer (EPMA-8050G). The specific surface area of the precursor was determined by the Brunauer-Emmett-Teller (BET) method with a Physisorption Analyzer (Anton Paar Nova 800). Thermal stability and decomposition behavior were evaluated using thermogravimetric analysis (TG) with a TG-DSC3+ STARe System (Mettler Toledo) at a heating rate of 5°C min^{-1} from 25 to 800°C. Additionally, the surface chemical states of elements were analyzed using X-ray photoelectron spectroscopy (XPS, Kratos Axis Supra) to provide insights into the surface composition and electronic structure of the materials.

2.3 Electrochemical Evaluation

To prepare the cathode electrodes, the active material, carbon black, and polyvinylidene fluoride (PVDF) were mixed in an 8:1:1 mass ratio to form a uniform slurry (Org et al., 2020). The mixture was then coated onto aluminum foil and dried at 80°C for four hours, followed by vacuum drying at 100°C for an additional four hours. Circular electrodes with a diameter of 12 mm were punched from the coated foil. The CR2032 coin cells were assembled in an argon-filled glove box, using lithium metal as the counter electrode. Galvanostatic charge-discharge cycling was conducted using a LAND-CT2001A battery testing system within a voltage range of 2.7–4.3 V (vs. Li/Li^+) at a current rate of 0.1 C. Electrochemical impedance spectroscopy (EIS) and cyclic voltammetry (CV) were performed using a CHI760E electrochemical workstation. EIS measurements were conducted over a frequency range of 10^{-2} to 10^6 Hz, while CV was recorded between 2.7 and 4.3 V at a scan rate of 10^{-3} mV s^{-1}.

3. RESULTS AND DISCUSSION

The NCM622 single-crystal samples (SC-0, SC-2.5, SC-3.75) were synthesized under varying N_2 : air conditions and subsequently analyzed using X-ray diffraction (XRD) to examine their crystalline structure. As shown in Figure 1(a), all samples exhibit prominent peaks corresponding to the R-3m space group, characteristic of the hexagonal α-$NaFeO_2$ structure (Chu et al., 2022). The clear separation of the (006)/(012) and (018)/(110) peaks indicates a well-ordered layered structure (Zhang et al., 2020). To further quantify the structural organization, Rietveld refinement was performed, and the results are presented in Figure 1(b–d). The calculated I(003)/I(104) and c/a ratios, summarized in Table 1, provide insights into the degree of Li^+/Ni^{2+} intermixing. The c/a ratio remained stable at 4.959 across all samples, confirming the preservation of the layered structure, while the $I_{(003)}/I_{(104)}$ ratio exhibited slight variations, with SC-2.5 achieving the highest value (1.344), suggesting improved cation ordering (Tian et al., 2020). The lattice volume (V) of SC-2.5 (100.91 $Å^3$) is slightly higher than that of SC-0 (100.85 $Å^3$) and SC-3.75 (100.80 $Å^3$), indicating a more relaxed crystal structure. The refinement parameters Rp/Rwp were lowest for SC-0 (1.55/2.08), indicating the best fit between the model and experimental data, while slightly

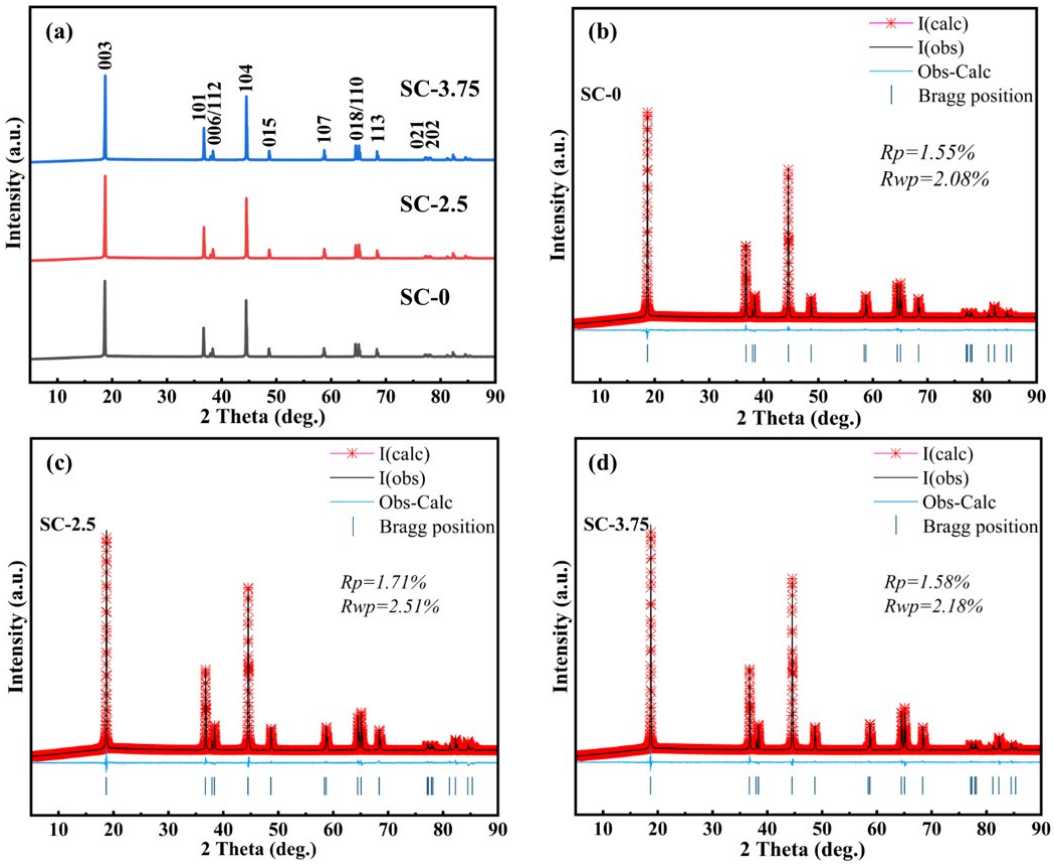

Figure 1. XRD Patterns (a), Rietveld Refinement Curves (b-d) of Cathodes

Table 1. The Results of The Rietveld Refinement and The $LiCoO_2$ Residual Testing of Cathodes

Sample Name	a (Å)	c (Å)	c/a	I(003)/I(104)	V (Å^3)	Rp (%)	Rwp (%)	Li_2CO_3 Residual (%)
SC-0	2.863	14.199	4.959	1.319	100.85	1.55	2.08	0.883
SC-2.5	2.864	14.204	4.959	1.344	100.91	1.71	2.51	0.533
SC-3.75	2.864	14.204	4.959	1.306	100.80	1.58	2.18	0.791

higher values were observed for SC-2.5 (1.71/2.51) and SC-3.75 (1.58/2.18). Additionally, the residual Li_2CO_3 content analysis showed that SC-2.5 had the lowest value (0.5331%), demonstrating that the sintering process under 2.5 μm air partitioning conditions effectively promoted single-crystal formation (Aktekin et al., 2024).

The morphology of the NCM622 precursors synthesized under different N_2 : air conditions was examined using SEM, as shown in Figure 2(a–c). The images reveal that HP-0 (Figure 2(a)) exhibits a loosely packed structure with weak interparticle cohesion, whereas HP-2.5 (Figure 2(b)) appears denser and more compact. In contrast, HP-3.75 (Figure 2(c)), although also dense, shows indications of fiber thinning. The particle size distribution of the precursors is centered around the target size of 5 μm. HP-0 and HP-3.75 display broader and lower peaks, indicating lower particle uniformity. In comparison, HP-2.5 shows a much narrower and sharper peak, reflecting a more uniform particle distribution. This observation is further supported by the span analysis in Table 2, where a span value closer to 0 and below 1 reflects greater homogeneity and uniformity (Hietaniemi et al., 2021). HP-2.5 achieved the best uniformity with a span value of 0.465, compared to 0.515 for HP-3.75 and 0.523 for HP-0.

To further analyze elemental distribution, EDS mapping was conducted, as illustrated in Figure 2(d–f). The Ni, Co, Mn, and O elements are uniformly distributed across all precursor particles, with no significant anomalies observed. This suggests that variations in oxygen dispersion have minimal impact on the elemental homogeneity of the materials. Additionally, cross-sectional SEM images (Figure 2(g–i)) provide further insights into the internal particle structure. All precursors exhibit well-defined nucleation, confirming successful particle

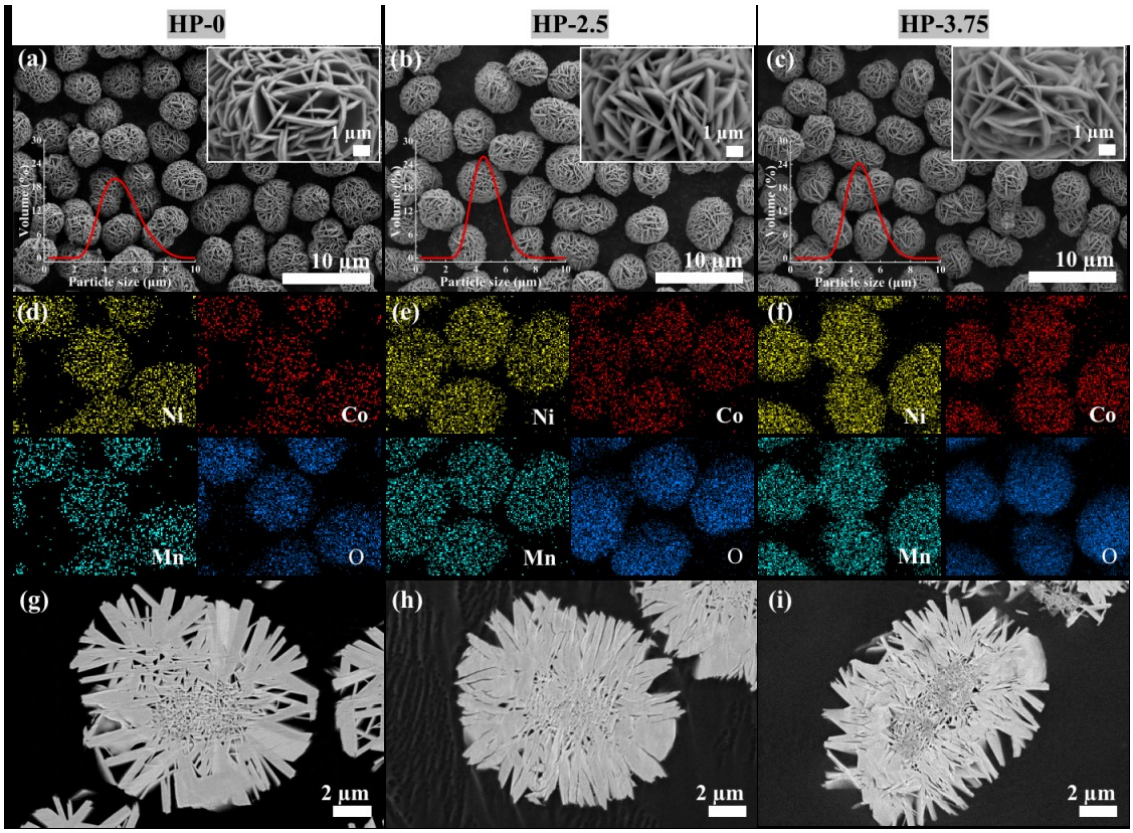

Figure 2. SEM Images (a-c), EDS Mapping (d-f), SEM Cross-Sectional Images (g-i) of Precursors

formation during synthesis. Specifically, HP-2.5 demonstrates a highly compact structure with a smooth and gradual particle development. In comparison, HP-0 displays a more loosely arranged fiber-like morphology, while HP-3.75 takes on a slightly elliptical shape with partially closed sections and internal cavities near the outermost surface.

Table 2. The Results of The Total Weight Loss, Span, TD, AD, and BET Tests of Precursors

Sample Name	Span $(D_{90} - D_{10})/D_{50}$	Total Weight Loss (%)	TD (g cm^{-3})	AD (g cm^{-3})	BET (m^2 g^{-1})
HP-0	0.523	16.93	1.521	1.091	5.370
HP-2.5	0.465	16.31	1.635	1.218	5.320
HP-3.75	0.515	16.67	1.558	1.112	9.250

The nucleation and dispersion of Ni, Co, and Mn examined using EPMA are illustrated in Figure 3(a-c). Each element distinctly exhibits ideal dispersion conditions when counts are used as an indicator. This acts as a standard for the successful synthesis of a good precursor. The air configuration influences the increase in element dispersion during nucleation and particle growth, as evidenced by the higher counts for each element overall in HP-2.5 and HP-3.75 when compared to HP-0. The effectiveness of the N_2 : air ratio of 2.4:0.2 at 2.5 μm is confirmed by the high Ni contrast, which reaches 237 at SC-2/5 with a dense formation. With Co counts of 95/96 and Mn counts of 115/119, HP-2.5 and HP-3.75 exhibit striking similarities.

Table 2 contains additional critical information about the function of structure and how it influences electrochemical performance. The TG-DTG test explains that two phases occur during temperature increase: dehydration and hydroxide decomposition. Hydroxide decomposition occurs above 300°C (the loss of metal hydroxide and the formation of NCM622 oxide), whereas dehydration occurs between 100°C and 200°C (Li et al., 2024). Because of the denser and more resilient particle condition, HP-2.5 maintains weight stability with a minimum value of 16.31%, calculated using the total weight loss percentage from both stages. HP-0, on the other hand, has a higher value of 16.93% due to increased interparticle cohesion. Higher TD and AD values generally indicate better cathode formation in terms of structure and morphology, as well as improved battery performance, based on precursor properties (Xia et al., 2018). Among the samples, HP-2.5 exhibits the highest values, with TD/AD of 1.635/1.218 g cm^{-3}, followed by HP-3.75 (1.558/1.112 g cm^{-3}) and HP-0 (1.521/1.091 g cm^{-3}). In addition, HP-2.5 shows the lowest BET surface area (5.320 m^2 g^{-1}), suggesting that a smaller

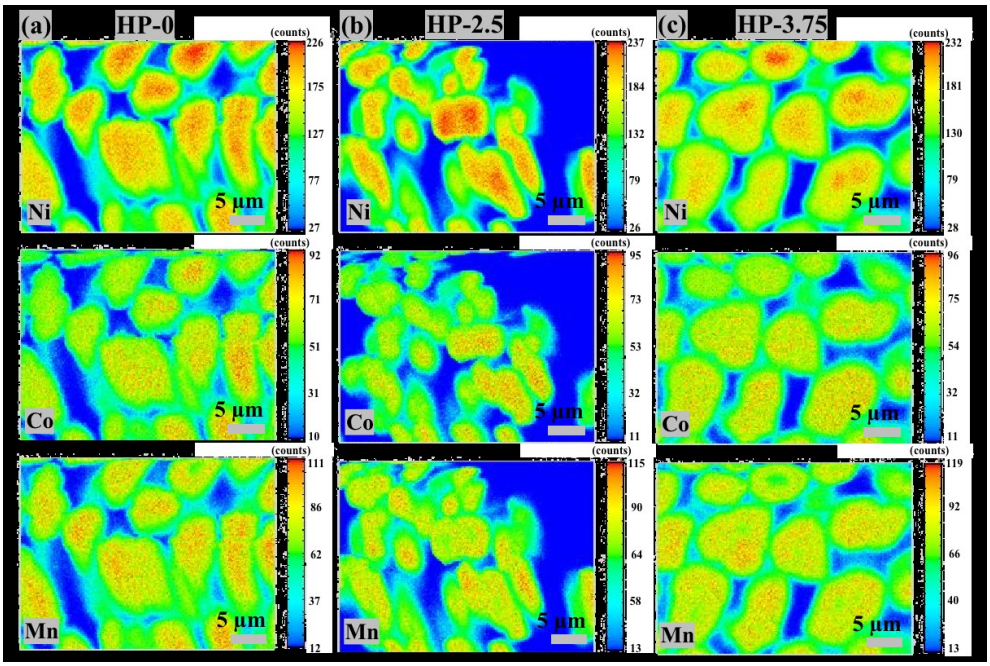

Figure 3. EPMA Image of Precursors

Table 3. The Results of The Electrochemical Performance of Single-Crystal NCM622 (1CE = 1st Cycle Coulombic Efficiency; 1DC = 1st Cycle Discharge Capacity; 100CE = 100th Cycle Coulombic Efficiency; 100DC = 100th Cycle Discharge Capacity; 100CR = 100th Cycle Capacity Retention; ΔE = Delta E of CV Analysis; R_F = Resistance of Film; and R_{CT} = Resistance of Charge Transfer)

Samplename	1CE(%)	1DC(mAh g^{-1})	100CE(%)	100DC(mAh g^{-1})	100CR(%)	ΔE(V)	R_F(Ω)	R_{CT} (Ω)
SC-0	86.87	161.04	99.50	126.50	84.60	0.212	50.6	112.4
SC-2.5	88.84	168.48	99.96	134.81	86.32	0.127	31.3	35.2
SC-3.75	86.61	162.94	99.64	130.27	85.61	0.146	49.5	57.5

surface area favors enhanced cathode formation, likely due to its compact morphology and limited particle interaction with air (0.2 at 2.5 μm).

The SEM images presented in Figure 4(a–c) confirm the successful formation of single-crystal NCM622 through the sintering process. Each sample exhibits well-defined single-crystal morphology, with particle sizes appearing nearly identical. However, the presence of residual Li_2CO_3, as discussed earlier, is consistent with the small agglomerations observed in SC-0, where lithium residue remains on the surface. SC-3.75, while showing a more consolidated structure, still demonstrates slight agglomeration tendencies. In contrast, SC-2.5 displays well-formed, clearly defined single-crystal particles with a smooth surface, indicating optimal sintering conditions. This highlights the importance of lithium mixing with precursors during the sintering process, which significantly influences crystalline structure and morphology (Xue et al., 2024). To further investigate the electronic structure and oxidation states of transition metals, XPS analysis was conducted, as shown in Figure 4(d–f). The Ni_2p spectra reveal that the Ni^{2+} / (Ni^{2+} + Ni^{2+}) ratio is highest in SC-2.5 (0.35%) compared to SC-0 (0.33%) and SC-3.75 (0.34%), with $Ni_2p_{3/2}$ peaks appearing in the typical 854-856 eV range. This suggests that SC-2.5 exhibits the optimal degree of cation mixing, which is closely linked to improved structural stability ratio (Ou et al., 2022). Similarly, the $Co_2p_{3/2}$ and $Mn_2p_{3/2}$ peaks, located at ~779-780 eV and ~643 eV, respectively, further validate the oxidation state distribution. SC-2.5 achieves the highest Co^{3+} (43%) and Mn^{4+} (50%) concentrations, surpassing SC-0 (41% and 49%) and SC-3.75 (42% and 50%). This suggests that SC-2.5 benefits from superior thermal stability and well-structured morphology, which could translate to enhanced electrochemical performance.

The electrochemical performance is shown in Figure 5(a–f) and Table 5. SC-2.5 has the highest initial discharge capacity and Coulombic efficiency (168.48 mAh g^{-1} and 88.84%, respectively) (Figure 5a). This is much higher than SC-0 (161.04 mAh g^{-1}, 86.87%) and SC-3.75 (162.94 mAh g^{-1}, 86.61%), showing that a well-optimized crystalline structure and single-crystal morphology are crucial to initial performance. Figure 5(b, c) shows that after 100 cycles, SC-2.5 remains stable with

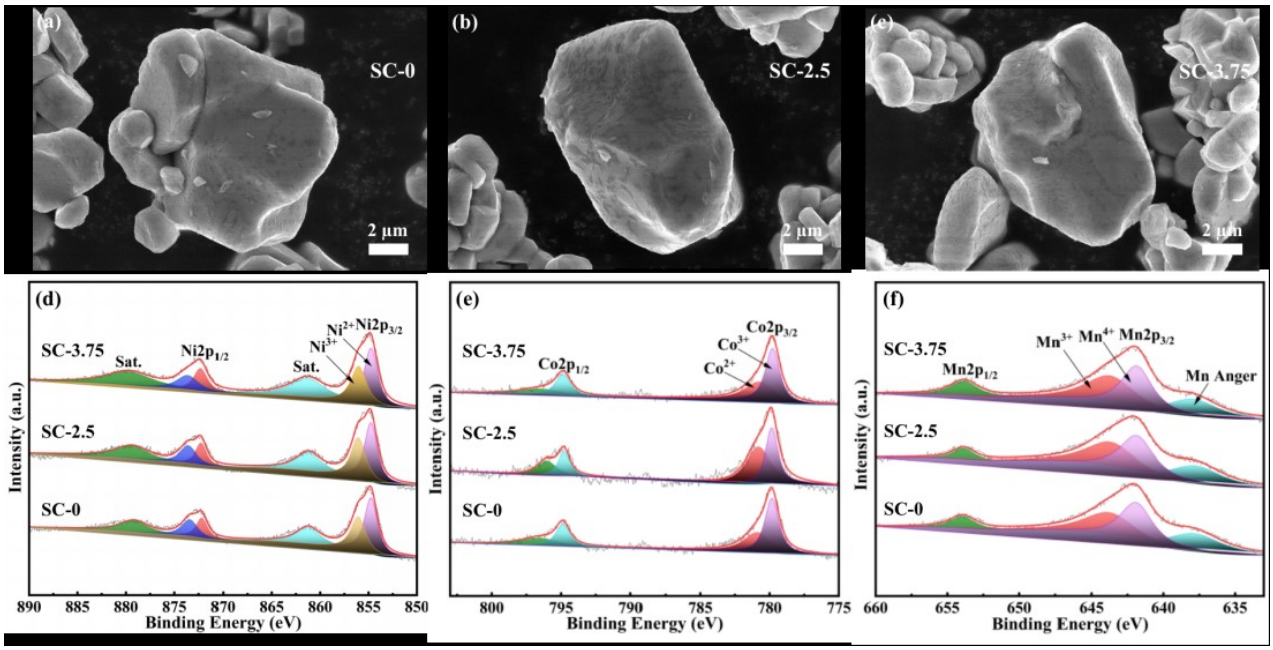

Figure 4. SEM Images (a-c), XPS Spectra of Ni_2p (d), Co_2p (e), Mn_2p (f) of Cathodes

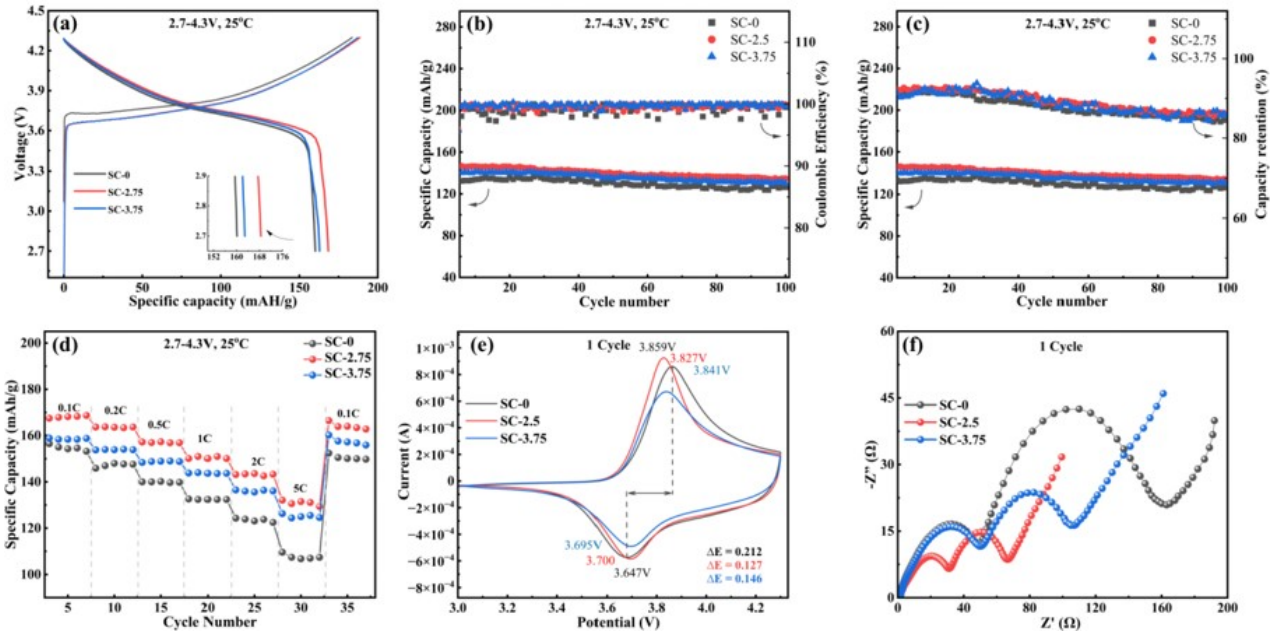

Figure 5. The Electrochemical Performance, Initial Charge-Discharge (a), Cycling Performance and Coulombic Efficiency (b), Cycling Performance and Capacity Retention (c), Rate Capability (d), Cyclic Voltammetry (CV) (e), and Electrochemical Impedance Spectroscopy (EIS) (f) of Cathodes

a low capacity fade of 19% (134.81 mAh g^{-1}), followed by SC-3.75 with 20% (130.27 mAh g^{-1}) and SC-0 with 21%. Additionally, Coulombic efficiency and capacity retention remain above 95% and 80%. SC-2.5 has the best Coulombic efficiency and capacity retention (134.81 mAh g^{-1} and 86.32%) over SC-0 and SC-3.75. After five cycles, capacity retention is highest at 0.1C and recovers when the current returns to 0.1C (Figure 5d). This trend continues with SC-2.5 outperforming SC-0 and SC-3.75.

The first cycle CV and EIS curves are shown in Figure 5(e, f). In Figure 5e, all reduction and oxidation peaks are clear and sharp, but SC-2.5 has the highest and sharpest. SC-2.5 has the lowest potential difference (ΔE) of 0.127 V, indicating a more efficient, stable, and reversible redox reaction, lead-

ing to better electrochemical performance. Thus, SC-2.5 has good conductivity, lower internal resistance, and better charge-discharge stability (Bouguern et al., 2024). In Figure 5f, the EIS analysis shows distinct impedance curves, with the Z' vs. -Z" plot showing two key resistances: R_F, the surface layer (SEI or reaction layer), and R_{CT}, the charge transfer resistance. RF and RCT are crucial for cycling stability and electrochemical performance, with lower values indicating better performance (Zhu et al., 2019). SC-2.5 has lower R_F (31.3 Ω) and R_{CT} (35.2 Ω) than SC-3.75, which has higher values (R_F = 50.6 Ω , R_{CT} = 112.4 Ω).

4. CONCLUSIONS

The core-shell condition established at N_2 : air during the synthesis of single-crystal NCM622 was effectively investigated and achieved. The condition of N_2 : air = 2.4 : 0.2 yielded crystals up to 2.5 μm, while N_2 : air = 2.4 : 0 formed crystals up to 5 μm, labeled as HP2.5/SC.2.5, exhibiting favorable crystalline structure, morphology, and correlation with electrochemical performance. The nucleation and growth of precursor particles were highly effective. The sintering stage (950°C/3 hours and 820°C/7 hours) effectively demonstrated the optimal conditions for the formation of single-crystal particles, resulting in an excellent single-crystal morphology characterized by a high I003/I104 ratio (1.344), an Rp of 1.71%, an Rwp of 2.51%, and a minimal residual Li_2Co_3 content (0.533). Consistent with the electrochemical findings, SC-2.5 exhibits the greatest contrast relative to SC-0 and SC-3.75, demonstrating an initial discharge capacity of 168.48 mAh g^{-1} and a Coulombic efficiency of 88.84%. After 100 cycles, the stability and performance results remain superior to SC-2.5. The discharge capacity of 134.81 mAh g^{-1} is notably high, with a capacity retention exceeding 85%, specifically 86.32%. The results indicate that the single-crystal half core-shell air framework positively influences the structural mechanism of the single-crystal NCM622.

5. ACKNOWLEDGEMENT

The author expresses gratitude to Central South University and GEM Co., Ltd. for their support in the writing of this article.

REFERENCES

Aktekin, B., A. E. Sedykh, K. Müller-Buschbaum, A. Henss, and J. Janek (2024). The Formation of Residual Lithium Compounds on Ni-Rich NCM Oxides: Their Impact on the Electrochemical Performance of Sulfide-Based ASSBs. *Advanced Functional Materials*, **34**(21); 2313252

Almafie, M. R., R. Dani, Riyanto, L. Marlina, J. Jauhari, and I. Sriyanti (2024). Preparation of PAN/PVDF Nanofiber Mats Loaded with Coconut Shell Activated Carbon and Silicon Dioxide for Lithium-Ion Battery Anodes. *Science and Technology Indonesia*, **9**(2); 427–447

Bouguern, M. D., A. K. M R, and K. Zaghib (2024). The Critical Role of Interfaces in Advanced Li-Ion Battery Technology: A Comprehensive Review. *Journal of Power Sources*, **623**; 235457

Chen, Y., Y. Kang, Y. Zhao, L. Wang, J. Liu, Y. Li, Z. Liang, X. He, X. Li, N. Tavajohi, and B. Li (2021). A Review of Li-Ion Battery Safety Concerns: The Issues, Strategies, and Testing Standards. *Journal of Energy Chemistry*, **59**; 83–99

Chu, R., Y. Zou, P. Zhu, S. Tan, F. Qiu, W. Fu, F. Niu, and W. Huang (2022). Progress of Single-Crystal Nickel-Cobalt-Manganese Cathode Research. *Energies*, **15**(23); 9235

Ding, H., X. Wang, J. Wang, H. Zhang, G. Liu, W. Yu, X. Dong, and J. Wang (2023). Morphology-Controllable Synthesis and Excellent Electrochemical Performance of Ni-Rich Layered NCM622 as Cathode Materials for Li-Ion Batteries via Glycerin-Assisted Solvothermal Method. *Journal of Power Sources*, **553**; 232307

Han, Y., Y. Lei, J. Ni, Y. Zhang, Z. Geng, P. Ming, C. Zhang, X. Tian, J. L. Shi, Y. G. Guo, and Q. Xiao (2022). Single-Crystalline Cathodes for Advanced Li-Ion Batteries: Progress and Challenges. *Small*, **18**(43); 2107048

Hietaniemi, M., T. Hu, J. Välikangas, J. Niittykoski, and U. Lassi (2021). Effect of Precursor Particle Size and Morphology on Lithiation of $Ni_{0.6}Mn_{0.2}Co_{0.2}(OH)_2$. *Journal of Applied Electrochemistry*, **51**(11); 1545–1557

Jo, C. H., N. Voronina, and S. T. Myung (2022). Single-Crystalline Particle Ni-Based Cathode Materials for Lithium-Ion Batteries: Strategies, Status, and Challenges to Improve Energy Density and Cyclability. *Energy Storage Materials*, **51**; 568–587

Kim, A. Y., F. Strauss, T. Bartsch, J. H. Teo, T. Hatsukade, A. Mazilkin, J. Janek, P. Hartmann, and T. Brezesinski (2019a). Stabilizing Effect of a Hybrid Surface Coating on a Ni-Rich NCM Cathode Material in All-Solid-State Batteries. *Chemistry of Materials*, **31**(23); 9664–9672

Kim, J. H., K. J. Park, S. J. Kim, C. S. Yoon, and Y. K. Sun (2019b). A Method of Increasing the Energy Density of Layered Ni-Rich Cathodes (x=0.05. 0.1. 0.2). *Journal of Materials Chemistry A*, **7**(6); 2694–2701

Li, H., L. Wang, Y. Song, Z. Zhang, A. Du, Y. Tang, J. Wang, and X. He (2024). Why the Synthesis Affects Performance of Layered Transition Metal Oxide Cathode Materials for Li-Ion Batteries. *Advanced Materials*, **36**(16); 2312292

Lu, Y., Y. Mo, Y. Chen, and F. Yu (2021). Effects of Various Elements Doping on $LiNi_{0.6}Co_{0.2}Mn_{0.2}O_2$ Layered Materials for Lithium-Ion Batteries. *Energy Technology*, **9**(7); 2100074

Luo, Q., W. Chen, and H. Fang (2022a). A Green and Economical Route to the Precursor for the Synthesis of Single Crystal $LiNi_{0.5}Co_{0.2}Mn_{0.3}O_2$. *Ceramics International*, **48**(12); 16737–16743

Luo, Y. H., H. X. Wei, L. B. Tang, Y. D. Huang, Z. Y. Wang, Z. J. He, C. Yan, J. Mao, K. Dai, and J. C. Zheng (2022b). Nickel-Rich and Cobalt-Free Layered Oxide Cathode Materials for Lithium Ion Batteries. *Energy Storage Materials*, **50**; 274–307

Org, W. E., B. He, G. Guo, N. Zhang, J. Wu, J. Zhu, and J. Qiu (2020). Study on the Preparation and Modification

of $LiNi_{0.6}Co_{0.2}Mn_{0.2}O_2$ from Spent Lithium Ion Batteries as Lithium and Cobalt Source. *International Journal of Electrochemical Science*, **15**; 6920–6929

Oswald, S., D. Pritzl, M. Wetjen, Y. Zhang, T. Hao, X. Huang, J. H. Choi, H. Kim, and J.-H. Lim (2022). Elucidating the Implications of Morphology on Fundamental Characteristics of Nickel-Rich NCMs: Cracking, Gassing, Rate Capability, and Thermal Stability of Poly- and Single-Crystalline NCM_{622}. *Journal of The Electrochemical Society*, **169**(5); 050501

Ou, L., S. Nong, R. Yang, Y. Li, J. Tao, P. Zhang, H. Huang, X. Liang, Z. Lan, H. Liu, D. Huang, J. Guo, and W. Zhou (2022). Multi-Role Surface Modification of Single-Crystalline Nickel-Rich Lithium Nickel Cobalt Manganese Oxides Cathodes with WO_3 to Improve Performance for Lithium-Ion Batteries. *Nanomaterials*, **12**(8); 1324

Tajik, M., A. Makui, and B. M. Tosarkani (2023). Sustainable Cathode Material Selection in Lithium-Ion Batteries Using a Novel Hybrid Multi-Criteria Decision-Making. *Journal of Energy Storage*, **66**; 107089

Tian, L., H. Yuan, Q. Shao, S. D. A. Zaidi, C. Wang, and J. Chen (2020). Synergistic Effect of $Li_2MgTi_3O_8$ Coating Layer with Dual Ionic Surface Doping to Improve Electrochemical Performance of $LiNi_{0.6}Co_{0.2}Mn_{0.2}O_2$ Cathode Materials. *Ionics*, **26**(10); 4937–4948

Weitong, Y., L. Ruifeng, C. Yue, S. Lijun, L. Xiaoying, and J. Qi (2023). Preparation of a High Performance $LiNi_{0.6}Co_{0.2}Mn_{0.2}O_2$ Cathode Material by Using Citric Acid as a Complexing Agent. *Green Chemistry*, **25**(3); 1085–1095

Xia, Y., J. Zheng, C. Wang, and M. Gu (2018). Designing Principle for Ni-Rich Cathode Materials with High Energy Density for Practical Applications. *Nano Energy*, **49**; 434–452

Xue, L., C. Tian, Y. Liu, X. Wen, T. Huang, and A. Yu (2024). Elucidating the Mechanical-Electrochemical Interactions in Single Crystalline $LiNi_{0.7}Co_{0.1}Mn_{0.2}O_2$ Cathode Material During Solid-State Calcination. *Ceramics International*, **50**(18); 31998–32006

Zhang, F., S. Lou, S. Li, Z. Yu, Q. Liu, A. Dai, C. Cao, M. F. Toney, M. Ge, X. Xiao, W. K. Lee, Y. Yao, J. Deng, T. Liu, Y. Tang, G. Yin, J. Lu, D. Su, and J. Wang (2020). Surface Regulation Enables High Stability of Single-Crystal Lithium-Ion Cathodes at High Voltage. *Nature Communications*, **11**(1); 1–11

Zhao, W., L. Zou, L. Zhang, X. Fan, H. Zhang, F. Pagani, E. Brack, L. Seidl, X. Ou, K. Egorov, X. Guo, G. Hu, S. Trabesinger, C. Wang, and C. Battaglia (2022). Assessing Long-Term Cycling Stability of Single-Crystal Versus Polycrystalline Nickel-Rich NCM in Pouch Cells with 6 $mAhcm^{-2}$ Electrodes. *Small*, **18**(14); 2107357

Zhu, B., Y. Ning, Z. Xu, G. Wei, and J. Qu (2024). Comparative Study of Polycrystalline and Single-Crystal NCM_{811} Cathode Materials: The Role of Crystal Defects in Electrochemical Performance. *Journal of Materials Chemistry A*, **12**(3); 1671–1684

Zhu, P., V. Trouillet, S. Heißler, and W. Pfleging (2023). Laser Structuring of High Mass Loaded and Aqueous Acid Processed $Li(Ni_{0.6}Mn_{0.2}Co_{0.2})O_2$ Cathodes for Lithium-Ion Batteries. *Journal of Energy Storage*, **66**; 107401

Zhu, Y., Y. Zhou, X. Tian, X. Huang, R. Yu, G. Wu, and G. Z. Chen (2019). Inter-Particle Electronic and Ionic Modifications of the Ternary Ni-Co-Mn Oxide for Efficient and Stable Lithium Storage. *Journal of The Electrochemical Society*, **166**(14); A3162–A3167

